Article

Design and Synthesis of TiO$_2$ Hollow Spheres with Spatially Separated Dual Cocatalysts for Efficient Photocatalytic Hydrogen Production

Qianqian Jiang [1], Li Li [1], Jinhong Bi [1,2,*], Shijing Liang [1,2,*] and Minghua Liu [1]

[1]   Department of Environmental Science and Engineering, Fuzhou University, Minhou 350108, China;
      jqq199207@163.com (Q.J.); lili@fjpsc.edu.cn (L.L.); mhliu2000@fzu.edu.cn (M.L.)
[2]   State Key Laboratory of Photocatalysis on Energy and Environment, Fuzhou University,
      Fuzhou 350002, China
*   Correspondence: bijinhong@fzu.edu.cn (J.B.); sjliang2012@fzu.edu.cn (S.L.); Tel.: +86-591-2286-6070 (J.B.)

Abstract: TiO$_2$ hollow spheres modified with spatially separated Ag species and RuO$_2$ cocatalysts have been prepared via an alkoxide hydrolysis–precipitation method and a facile impregnation method. High-resolution transmission electron microscopy studies indicate that Ag species and RuO$_2$ co-located on the inner and outer surface of TiO$_2$ hollow spheres, respectively. The resultant catalysts show significantly enhanced activity in photocatalytic hydrogen production under simulated sunlight attributed to spatially separated Ag species and RuO$_2$ cocatalysts on TiO$_2$ hollow spheres, which results in the efficient separation and transportation of photogenerated charge carriers.

1. Introduction

Semiconductor photocatalysis as a green technology has attracted much interest for the application in solving environmental pollution and energy shortage [1–5]. Since the photolysis of water to produce hydrogen was discovered, TiO$_2$ has been most investigated in photocatalysis due to the chemical stability, nontoxicity, and low price [5–8]. However, the drawbacks of TiO$_2$, such as the low utilization of sunlight, the rapid recombination of the photogenerated charges, and few suitable active sites, extremely limit photocatalytic performance. Tuning the morphology and structure of TiO$_2$ with expectations of achieving novel or enhanced properties have been regarded as an efficient way to overcome the drawbacks—for instance, the fabrication of TiO$_2$ nanospheres, nanorods, nanowires, and nanobelts [9–13]. Especially, the submicron-scale hollow spheres of TiO$_2$ are promising because they can provide large specific surface areas and enhance light scattering properties and their inner and outer surfaces can be controlled and selectively functionalized [14]. Moreover, the photocatalytic properties of TiO$_2$ hollow spheres can be modified by loading cocatalysts [15–17], which can serve as reaction sites and provide the trapping sites for the photogenerated carriers of the surface. The internal electric field can be formed between the cocatalyst and the photocatalyst due to the different Fermi level, which can promote the directional migration of photogenerated electrons and holes and prohibit the recombination of the photogenerated carriers [18].

The space locations of the cocatalysts loaded on the photocatalytic materials can greatly affect the migration of the photogenerated carriers and then further affect the photocatalytic activity. The oxidation cocatalyst and reduction cocatalyst loaded on different spatial locations of the photocatalysts may produce spatially separated reaction sites with oxidizing and reducing abilities, respectively, which consequently lead to the directional migration of photogenerated electrons and

holes and thus prohibit the recombination of photogenerated carriers. Domen et al. have demonstrated that SiO_2/Ta_3N_5 core/shell structures with spatially separated cocatalysts show superior photocatalytic activity [19]. Li et al. have reported that reduction cocatalysts (MoS_2, NiS, WS_2, etc.) and oxidation cocatalysts (IrO_x, MnO_x, RuO_x, etc.) can be selectively deposited on the (010) and (110) facets of $BiVO_4$, respectively, which results in much higher photocatalytic activity compared to that with randomly distributed cocatalysts [20,21]. In general, the noble metals (Au, Ag, Pt, Pd, etc.), MoS_2, and graphene exhibiting superior electron mobility often act as reduction cocatalysts to improve the efficiency of photoproduction electron migration [7,22–25]. The cocatalysts such as RuO_2, IrO_2, CoO_x, and MnO_x can act as hole collector [26–29]. Loading the reduction and oxidation catalysts on the inner and outer surfaces of TiO_2 hollow spheres can be expected to achieve enhanced photocatalytic activity.

Herein, we report a facile synthesis of TiO_2 hollow spheres modified with spatially separated Ag species and RuO_2 on the inner and outer surfaces of the TiO_2 hollow spheres (as shown in Scheme 1), which exhibited enhanced photocatalytic hydrogen production under solar light irradiation.
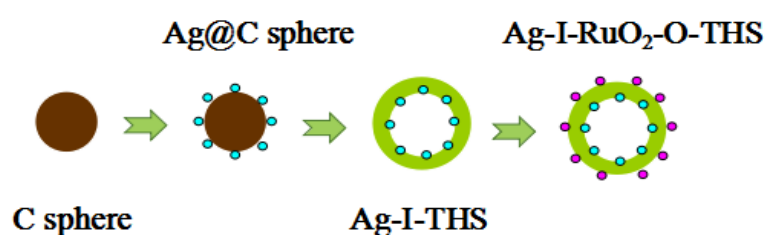
Scheme 1. Processes involved in the formation of dual cocatalysts co-loading on the TiO_2 hollow spheres (THS).

2. Experimental Section

2.1. Preparation of Catalysts

2.1.1. Synthesis of Carbon Spheres (C Sphere)

In a typical synthesis of carbon spheres, glucose (6 g) was dissolved into deionized water (60 mL) to form a clear solution and then was transferred into a 100 mL Teflon-lined autoclave and was reacted at 180 °C for 12 h. The obtained brown product was collected and washed with deionized water and ethanol and then dried at 80 °C. Finally, carbon spheres (denoted as C sphere) were obtained [30].

2.1.2. Synthesis of TiO_2 Hollow Spheres (THS)

An amount of 0.4 g of C sphere was added to 30 mL of pure ethyl alcohol. The obtained suspended solution was stirred for 30 min and then was dispersed under ultrasonic conditions for 30 min. Then, a solution consisting of 70 mL of pure ethyl alcohol, 0.2 g of hexadecyl trimethyl ammonium bromide (CTAB), and 0.6 mL of deionized water was added and stirred for 2 h. After that, 23 mL of a tetrabutyl titanate ethanol solution was added dropwise while stirring. The obtained suspended solution was transferred into the three-necked flask. After the reflux condensation at 85 °C for 100 min, the prepared product was collected, washed with deionized water and ethyl alcohol, and dried at 60 °C. The dried powders were further calcined at 500 °C for 2 h with a ramping rate of 2 °C/min and TiO_2 hollow spheres were then obtained and are denoted as THS [30].

2.1.3. Synthesis of Ag-Loaded TiO_2 Hollow Spheres on the Inner Surface (Ag-I-THS)

The loading Ag on the inner surface of THS included two steps. In the first step, Ag-loaded C sphere was prepared by an impregnation method [31]. An amount of 0.4 g of the above synthesized carbon spheres were impregnated in a 0.4 mL silver nitrate solution (10 mg/mL) and then dried at 80 °C for 2 h. The resulting powders were reduced by excess $NaBH_4$ solution (0.1 M). The obtained

product was washed with deionized water and ethanol and dried at 60 °C. Finally, the Ag-loaded carbon sphere powders (denoted as Ag@C sphere) were obtained. The second step was similar to the synthesis of THS except that 0.4 g of C sphere was replaced by 0.4 g of Ag@C sphere in this process. After the treatment, the Ag-loaded TiO_2 hollow spheres on the inner surface were obtained and are denoted as Ag-I-THS.

2.1.4. Synthesis of Ag- and RuO_2-Co-Loaded TiO_2 Hollow Spheres on the Inner Surface and Outer Surface (Ag-I-RuO_2-O-THS)

The above synthesized Ag-I-THS (0.2 g) was impregnated in a 0.2 mL ruthenium chloride solution (10 mg/mL) and then dried at 80 °C for 2 h. The resulting powders were calcined at 350 °C for 1 h, and Ag- and RuO_2-co-loaded TiO_2 hollow spheres on the inner surface and outer surface, respectively, were finally obtained and are denoted as Ag-I-RuO_2-O-THS.

2.1.5. Synthesis of RuO_2-Loaded TiO_2 Hollow Spheres on the Outer Surface (RuO_2-O-THS)

The loading of RuO_2 on the outer surface of THS was also conducted by an impregnation process [31]. The above synthesized THS (0.4 g) was impregnated in a 0.4 mL ruthenium chloride solution (10 mg/mL) and then dried at 80 °C for 2 h. The resulting powders were calcined at 350 °C for 1 h, and RuO_2-loaded TiO_2 hollow spheres on the outer surface were finally obtained and are denoted as RuO_2-O-THS [32].

2.1.6. Synthesis of RuO_2- and Ag-Co-Loaded TiO_2 Hollow Spheres on the Inner Surface and Outer Surface (RuO_2-I-Ag-O-THS)

The loading of RuO_2 and Ag on the inner surface and outer surface of THS included three steps. In the first step, RuO_2-loaded carbon spheres were prepared by an impregnation method [31]. An amount of 0.4 g of the above synthesized carbon spheres were impregnated in a 0.4 mL ruthenium chloride solution (10 mg/mL) and then dried at 80 °C for 2 h. The resulting powders were calcined at 350 °C for 1 h, and the RuO_2-loaded carbon sphere powders (denoted as RuO_2@C sphere) were finally obtained. The second step was similar to the synthesis of THS, except that the 0.4 g of carbon spheres were replaced by 0.4 g of RuO_2@C sphere in this process. After the treatment, the RuO_2-loaded TiO_2 hollow spheres on the inner surface were obtained and are denoted as RuO_2-I-THS. In the final step, the above synthesized RuO_2-I-THS (0.2 g) was impregnated in a 0.2 mL silver nitrate solution (10 mg/mL) and then dried at 80 °C for 2 h. The resulting powders were reduced by excess $NaBH_4$ solution (0.1 M). The obtained product was washed with deionized water and ethanol and dried at 60 °C. Finally, RuO_2- and Ag-co-loaded TiO_2 hollow spheres on the inner surface and outer surface, respectively, were obtained and are denoted as RuO_2-I-Ag-O-THS.

2.2. Characterizations

The as-prepared samples were characterized by powder X-ray diffraction (PXRD) on a Rigaku Mini Flex 600 X-ray diffractometer (Rigaku, Akishima, Japan) operated at 40 kV and 15 mA with Ni-filtered Cu Kα irradiation (λ = 1.5406 Å). Solid-state UV-Vis diffuse reflectance spectra (UV-Vis DRS) were obtained by using a UV-Vis spectrophotometer (Varian, Cary 500, Palo Alto, CA, USA). Barium sulfate was used as a reference. The Brunauer–Emmett–Teller (BET) surface area was measured with an ASAP2020 apparatus (Micromeritics, Atlanta, GA, USA). The transmission electron microscopy (TEM) images were recorded using a JEOL model JEM 2010 EX microscope (FEI, Hillsboro, OR, USA) at an accelerating voltage of 200 kV. X-ray photoelectron spectroscopy (XPS) measurements were performed on a PHI Quantum 2000 XPS system (Physical electronics, Portland, OR, USA) with a monochromatic Al KR source and a charge neutralizer. All binding energies were referenced to the C 1s peak (284.6 eV) of the surface adventitious carbon.

2.3. Photocatalytic Activity Evaluation

Photocatalytic hydrogen evolution from water-splitting reaction was carried out with powder samples to provide sufficient surface area in a glass-closed gas-circulation system and a 100 mL Pyrex glass reaction vessel. The reaction was performed by dispersing 80 mg of catalysts into an aqueous solution (80 mL) containing EDTA-2Na (0.5 g) as a sacrificial electron donor. The whole reaction system was evacuated to completely remove air before irradiation. During the experiment, a 300 W Xe lamp was employed as the light source to simulate sunlight. The incident photon flux is 3.4×10^{18} s^{-1}·cm^{-2}, and the irradiance intensity is 132.4 mW·cm^{-2}. The temperature of the reactant solution was kept at a constant temperature by a flow of cooling water during the reaction. The amount of H$_2$ evolution was analyzed by using an on-line gas chromatograph (Shimadzu, GC-8A, Kyoto, Japan) with a thermal conductivity detector (TCD) and using argon as the carrier gas. To evaluate the stability of the photocatalyst, the photocatalytic reactions were carried out as the similar procedure above by using 80 mg of catalysts for a total of 25 h with evacuation every 5 h.

3. Results and Discussion

3.1. Crystal Structure

The XRD patterns of TiO$_2$ hollow spheres showed a mixture of anatase and rutile TiO$_2$ (Figure 1). The diffraction peak located at 25.3° was attributed to (101) plane of anatase phase, while the diffraction peak located at 27.4° and 36.1° was attributed to (110) and (101) planes of rutile phase [33]. No significant peaks indicative of silver and ruthenium oxide were observed in the cocatalyst-loaded THS, which could be attributed to the very low content and/or high dispersion.
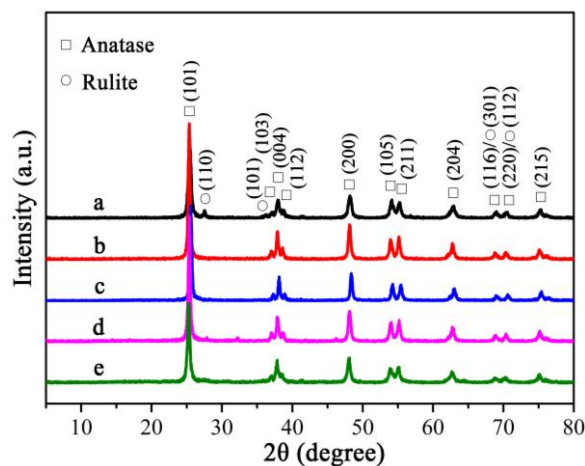

Figure 1. X-ray diffraction (XRD) patterns of TiO$_2$ hollow spheres (THS) loaded by the cocatalysts with different spatial dispersion: (**a**) THS; (**b**) Ag-loaded THS on the inner surface (Ag-I-THS); (**c**) RuO$_2$-loaded THS on the outer surface (RuO$_2$-O-THS); (**d**) Ag- and RuO$_2$-co-loaded THS on the inner surface and outer surface (Ag-I-RuO$_2$-O-THS); (**e**) RuO$_2$- and Ag-co-loaded THS on the inner surface and outer surface (RuO$_2$-I-Ag-O-THS).

3.2. BET Analyses

The BET surface areas and pore structures of THS and Ag-I-RuO$_2$-O-THS were evaluated by N$_2$ adsorption at 77 K. The pure THS and sample Ag-I-RuO$_2$-O-THS displayed type IV N$_2$ adsorption–desorption isotherms, corresponding to the mesoporous structure (Figure 2). The BET surface area of THS and Ag-I-RuO$_2$-O-THS samples were 34.5 m^2/g and 8.7 m^2/g, respectively. Compared with that of THS, the specific surface area of Ag-I-RuO$_2$-O-THS was obviously decreased, which may be because the loading of Ag and RuO$_2$ blocked off the pores of THS [34].
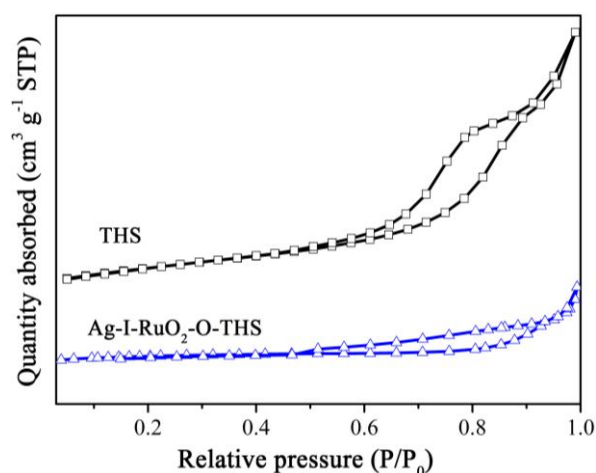
Figure 2. N_2 adsorption-desorption isotherms of THS and $Ag-I-RuO_2-O-THS$.

3.3. TEM Analyses

The morphology of $Ag-I-RuO_2-O-THS$ and the different spatial distribution of the cocatalysts were investigated by TEM. TEM image of $Ag-I-RuO_2-O-THS$ clearly elucidated the hollow structure by the striking contrast between the center and the edge with a diameter of ca. 200 nm and a shell thickness of ca. 20 nm (Figure 3a). The HRTEM image (Figure 3b) showed clear lattice fringes. The fringes of $d = 0.25$ nm and 0.32 nm matched well with that of the (101) and (110) crystallographic plane of rutile TiO_2 and the fringes located at 0.35 nm corresponded to that of (101) crystallographic plane of anatase TiO_2, which were in accordance with the result of XRD. Noteworthy, the (111) crystallographic plane of Ag_2O ($d = 0.27$ nm) and the (111) crystallographic plane of RuO_2 ($d = 0.28$ nm) can be observed on the inner surface and outer surface of TiO_2 hollow spheres, respectively, indicating the spatially separated dual cocatalysts loaded TiO_2 hollow spheres has been synthesized successfully.
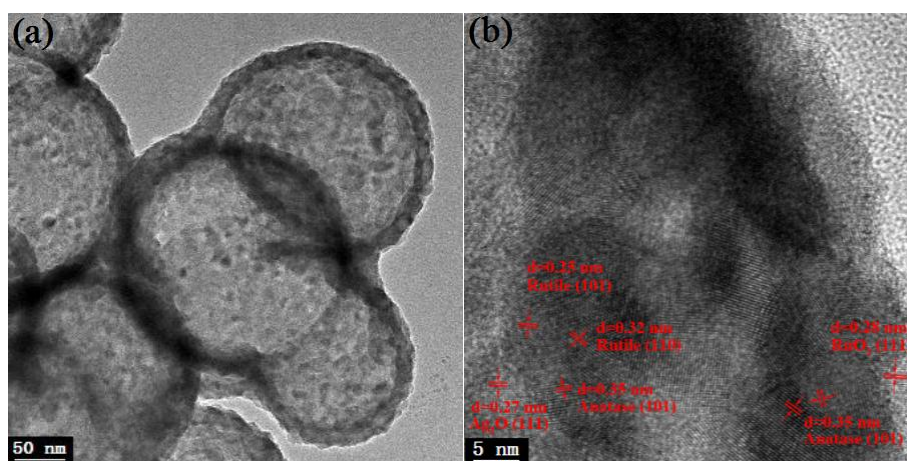

Figure 3. (**a**) Transmission electron microscopy (TEM) and (**b**) High resolution transmission electron microscopy (HRTEM) images of $Ag-I-RuO_2-O-THS$.

3.4. XPS Analyses

The chemical components and the states of C, Ru, Ag, O, and Ti in the $Ag-I-RuO_2-O-THS$ were investigated by XPS. As observed in Figure 4a, there are four peaks at about 284.6 eV, 285.2 eV, 286.6 eV, and 288.5 eV in the C 1s spectrum corresponding to the additional carbon, the residual carbon in C sphere, tetrabutyl titanate, and CTAB, respectively. Furthermore, the binding energy of Ru $3d_{3/2}$

was overlapped by that of C 1s; thus, the Ru oxidation state was evaluated from the Ru $3d_{5/2}$. The Ru $3d_{5/2}$ peak was located at 280.3 eV, which indicated the existence of Ru^{4+}, as expected for RuO_2 [35]. Figure 4b demonstrated the high-resolution XPS spectra for Ag $3d_{3/2}$ and Ag $3d_{5/2}$ located at 373.3 eV and 367.3 eV, respectively, corresponding to Ag^+ of Ag_2O [36]. The O 1s peak may be fitted into two peaks at 529.9 eV and 531.6 eV (Figure 4c), corresponding to the crystal lattice oxygen and the surface hydroxyl groups, respectively [37]. Meanwhile, the Ti 2p XPS spectra are deconvoluted into two peaks at 458.6 eV and 464.3 eV, corresponding to Ti^{4+} in TiO_2 [38] (Figure 4d).
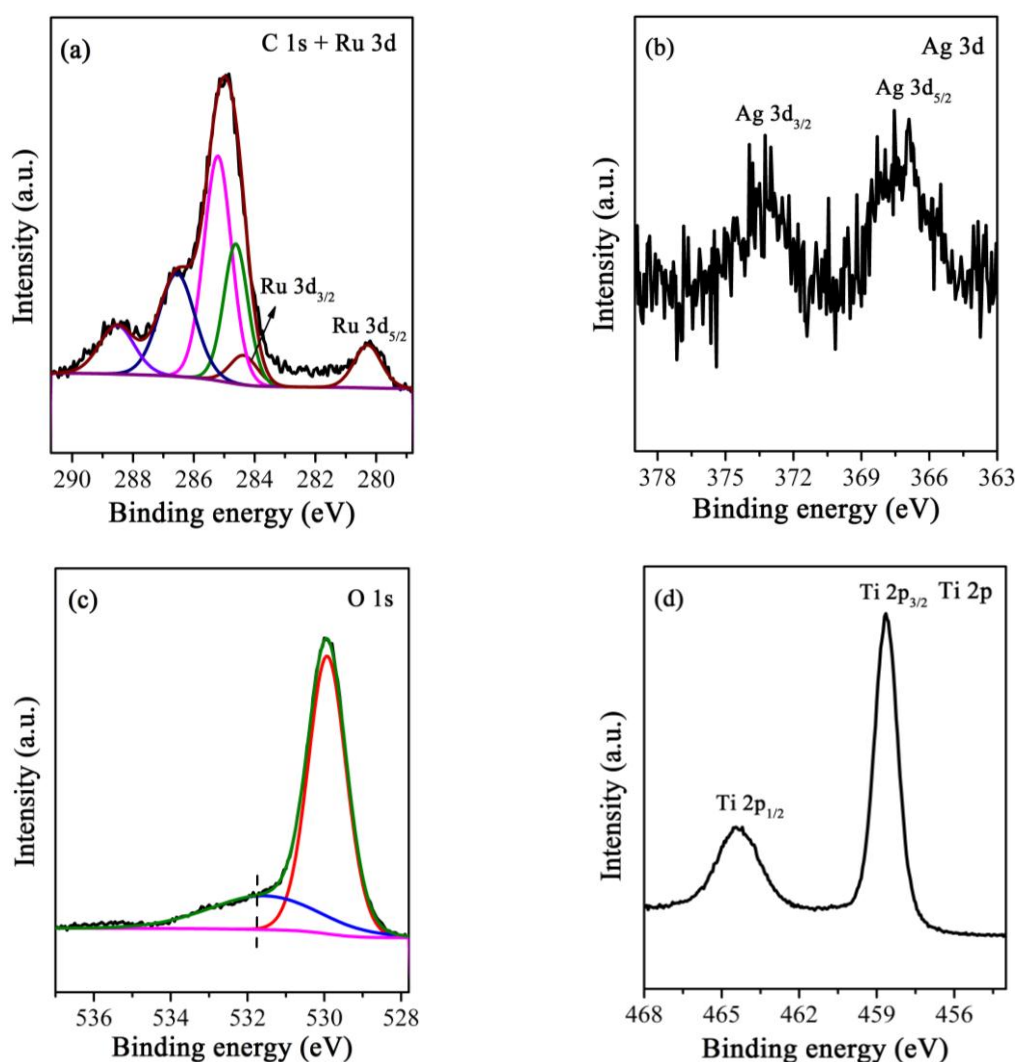

Figure 4. X-ray photoelectron spectroscopy (XPS) spectra of Ag-I-RuO_2-O-THS: (**a**) C 1s and Ru 3d; (**b**) Ag 3d; (**c**) O 1s; (**d**) Ti 2p.

3.5. UV-Vis DRS Analyses

As shown in the UV-Vis diffuse reflectance spectra, all samples displayed a similar band edge with a value of 3.3 eV, indicating that the photo-absorption properties of TiO_2 were maintained (Figure 5). TiO_2 absorbed only UV light, while the RuO_2-O-THS, Ag-I-RuO_2-O-THS, and RuO_2-I-Ag-O-THS exhibited a stronger light absorption in the visible light region owing to the presence of RuO_2. Compared to the other samples, RuO_2-I-Ag-O-THS composite displayed the characteristic localized surface plasmon resonance peak of Ag located at ca. 530 nm [39].
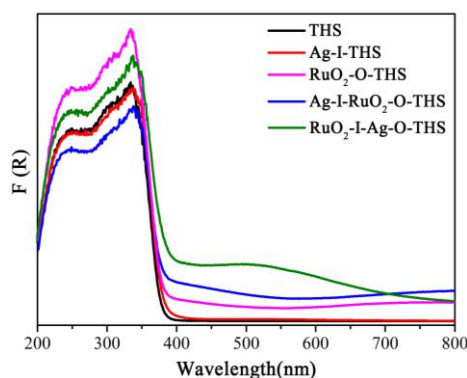
Figure 5. Ultraviolet-visible diffuse reflectance spectra (UV-Vis DRS) of THS loaded by the cocatalysts with different spatial dispersion.

3.6. Photocatalytic Activities

Figure 6 showed the photocatalytic activity of H_2 evolution of THS loaded with different spatial distribution of the cocatalysts within 5 h. The original TiO_2 hollow spheres produced a little amount of H_2. When Ag species and RuO_2 were loaded on TiO_2 hollow spheres, the activity of photocatalytic hydrogen production was greatly improved. The hydrogen yields of Ag-I-THS, RuO_2-O-THS, RuO_2-I-Ag-O-THS, and Ag-I-RuO_2-O-THS were 15.4, 139.0, 103.4, and 300.2 μmol, respectively. The H_2 evolution of Ag-I-RuO_2-O-THS was about 19.5 times over Ag-I-THS, 2.2 times over RuO_2-O-THS, and 2.9 times over RuO_2-I-Ag-O-THS. The results demonstrated that photocatalytic hydrogen production activity was enhanced by co-loading Ag species and RuO_2 on the inner and outer surfaces of THS. The stability of the photocatalysts is important for their applications. Thus, the stability of Ag-I-RuO_2-O-THS was investigated. As shown in Figure 7, the photocatalytic activity of Ag-I-RuO_2-O-THS increased with the increment of the photocatalytic reaction cycles. After three cycles, the hydrogen production tended to be a stable value. The increased amount of hydrogen may be due to the change of the chemical state of silver species under solar light irradiation [36,40]. As the reaction proceeds, the oxidation state of silver species can be gradually reduced to metallic silver, thus increasing photogenerated electrons mobility and significantly improving the hydrogen production. Scheme 2 shows the probable reaction mechanism for the photocatalytic water splitting reaction on Ag-I-RuO_2-O-THS. The oxidation cocatalyst RuO_2 and reduction cocatalyst Ag loaded on the outer and inner surface of THS can lead to the directional migration of photogenerated holes and electrons, which can prohibit the recombination of the photogenerated carriers and finally enhance the photocatalytic activity [21].
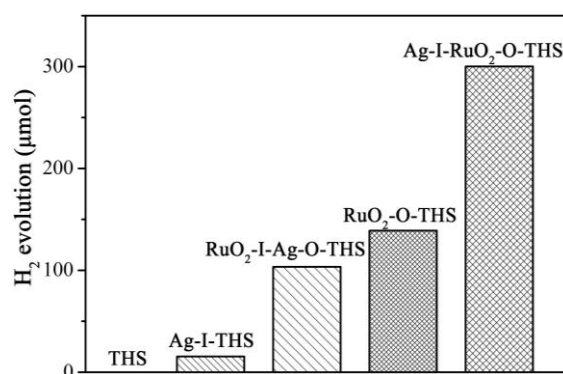

Figure 6. Photocatalytic activities of H_2 evolution on THS loaded by the cocatalysts with different spatial dispersion.
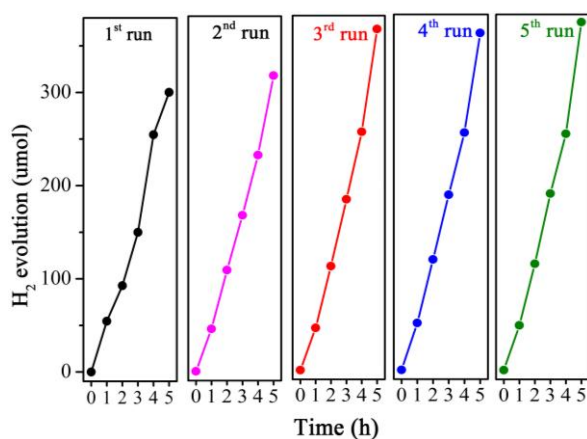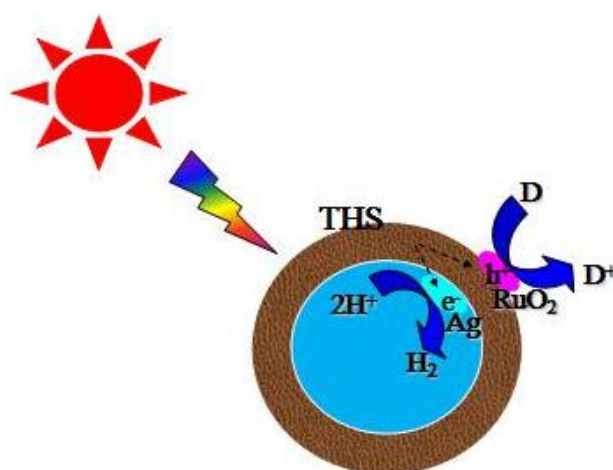
Figure 7. Stability of Ag-I-RuO$_2$-O-THS during prolonged photocatalytic operation.

Scheme 2. The photocatalytic hydrogen production on Ag-I-RuO$_2$-O-THS.

4. Conclusions

We have successfully synthesized TiO$_2$ hollow spheres modified with Ag species and RuO$_2$ on the inner and outer surfaces, respectively, via an alkoxide hydrolysis-precipitation method combined with a facile impregnation method. The as-obtained TiO$_2$ hollow spheres exhibited enhanced photocatalytic hydrogen production activity under solar light irradiation, which is ascribed to the effective transfer and separation of the photogenerated charge carriers at the interface, resulting from the suitable spatial separation of Ag species and RuO$_2$ cocatalysts on TiO$_2$ hollow spheres.

Author Contributions: Jinhong Bi and Shijing Liang conceived and designed the experiments; Li Li performed the experiments; Li Li and Qianqian Jiang analyzed the data and wrote the paper; Minghua Liu contributed reagents/materials/equipment.

Conflicts of Interest: The authors declare no conflict of interest.

References

1.　Chen, X.; Shen, S.; Guo, L.; Mao, S. Semiconductor-based photocatalytic hydrogen generation. *Chem. Rev.* **2010**, *110*, 6503–6570. [CrossRef] [PubMed]

2. Liu, H.; Yuan, J.; Shangguan, W.; Teraoka, Y. Visible-light-responding BiYWO$_6$ solid solution for stoichiometric photocatalytic water splitting. *J. Phys. Chem. C* **2008**, *112*, 8521–8523. [CrossRef]

3. Shimura, K.; Yoshida, T.; Yoshida, H. Photocatalytic activation of water and methane over modified gallium oxide for hydrogen production. *J. Phys. Chem. C* **2010**, *114*, 11466–11474. [CrossRef]

4. Zong, X.; Wu, G.; Yan, H.; Ma, G.; Shi, J.; Wen, F.; Wang, L.; Li, C. Photocatalytic H$_2$ evolution on MoS$_2$/CdS catalysts under visible light irradiation. *J. Phys. Chem. C* **2010**, *114*, 1963–1968. [CrossRef]

5. Fujishima, A. Electrochemical photolysis of water at a semiconductor electrode. *Nature* **1972**, *238*, 37–38. [CrossRef] [PubMed]

6. Xu, H.; Reunchan, P.; Ouyang, S.; Tong, H.; Umezawa, N.; Kako, T.; Ye, J. Anatase TiO$_2$ single crystals exposed with high-reactive {111} facets toward efficient H$_2$ evolution. *Chem. Mater.* **2013**, *25*, 405–411. [CrossRef]

7. Xiang, Q.; Yu, J.; Jaroniec, M. Synergetic effect of MoS$_2$ and graphene as cocatalysts for enhanced photocatalytic H$_2$ production activity of TiO$_2$ nanoparticles. *J. Am. Chem. Soc.* **2012**, *134*, 6575–6578. [CrossRef] [PubMed]

8. Hernández-Alonso, M.; Fresno, F.; Suárez, S.; Coronado, J. Development of alternative photocatalysts to TiO$_2$: Challenges and opportunities. *Energy Environ. Sci.* **2009**, *2*, 1231–1257. [CrossRef]

9. Kim, Y.; Lee, M.; Kim, H.; Lim, G.; Choi, Y.; Park, N.; Lee, W. Formation of highly efficient dye-sensitized solar cells by hierarchical pore generation with nanoporous TiO$_2$ spheres. *Adv. Mater.* **2009**, *21*, 3668–3673. [CrossRef]

10. Liu, B.; Aydil, E. Growth of oriented single-crystalline rutile TiO$_2$ nanorods on transparent conducting substrates for dye-sensitized solar cells. *J. Am. Chem. Soc.* **2009**, *131*, 3985–3990. [CrossRef] [PubMed]

11. Hoang, S.; Berglund, S.; Hahn, N.; Bard, A.; Mullins, C. Enhancing visible light photo-oxidation of water with TiO$_2$ nanowire arrays via cotreatment with H$_2$ and NH$_3$: Synergistic effects between Ti^{3+} and N. *J. Am. Chem. Soc.* **2012**, *134*, 3659–3662. [CrossRef] [PubMed]

12. Zhou, W.; Yin, Z.; Du, Y.; Huang, X.; Zeng, Z.; Fan, Z.; Zhang, H. Synthesis of few-layer MoS$_2$ nanosheet-coated TiO$_2$ nanobelt heterostructures for enhanced photocatalytic activities. *Small* **2013**, *9*, 140–147. [CrossRef] [PubMed]

13. Shin, W.; Lee, H.; Sohn, Y.; Shin, W. Novel inkjet droplet method generating monodisperse hollow metal oxide micro-spheres. *Chem. Eng. J.* **2016**, *292*, 139–146. [CrossRef]

14. Zhang, P.; Li, A.; Gong, J. Hollow spherical titanium dioxide nanoparticles for energy and environmental applications. *Particuology* **2015**, *22*, 13–23. [CrossRef]

15. Yu, Y.; Cao, C.; Chen, Z.; Liu, H.; Li, P.; Dou, Z.; Song, W. Au nanoparticles embedded into the inner wall of TiO$_2$ hollow spheres as a nanoreactor with superb thermal stability. *Chem. Commun.* **2013**, *49*, 3116–3118. [CrossRef] [PubMed]

16. Du, J.; Qi, J.; Wang, D.; Tang, Z. Facile synthesis of Au@TiO$_2$ core-shell hollow spheres for dye-sensitized solar cells with remarkably improved efficiency. *Energy Environ. Sci.* **2012**, *5*, 6914–6918. [CrossRef]

17. Li, A.; Zhang, P.; Chang, X.; Cai, W.; Wang, T.; Gong, J. Gold nanorod@TiO$_2$ yolk-shell nanostructures for visible-light-driven photocatalytic oxidation of benzyl alcohol. *Small* **2015**, *11*, 1892–1899. [CrossRef] [PubMed]

18. Yang, J.; Wang, D.; Han, H.; Li, C. Roles of cocatalysts in photocatalysis and photoelectrocatalysis. *Acc. Chem. Res.* **2013**, *46*, 1900–1909. [CrossRef] [PubMed]

19. Wang, D.; Hisatomi, T.; Takata, T.; Pan, C.; Katayama, M.; Kubota, J.; Domen, K. Core/shell photocatalyst with spatially separated co-catalysts for efficient reduction and oxidation of water. *Angew. Chem. Int. Ed.* **2013**, *52*, 11252–11256. [CrossRef] [PubMed]

20. Bai, S.; Yin, W.; Wang, L.; Li, Z.; Xiong, Y. Surface and interface design of cocatalysts toward photocatalytic water splitting and CO$_2$ reduction. *RSC Adv.* **2016**, *6*, 57446–57463. [CrossRef]

21. Li, R.; Zhang, F.; Wang, D.; Yang, J.; Li, M.; Zhu, J.; Zhou, X.; Han, H.; Li, C. Spatial separation of photogenerated electrons and holes among {010} and {110} crystal facets of BiVO$_4$. *Nat. Commun.* **2013**, *4*, 1432. [CrossRef] [PubMed]

22. Zhang, N.; Liu, S.; Fu, X.; Xu, Y. Synthesis of M@TiO$_2$ (M = Au, Pd, Pt) core-shell nanocomposites with tunable photoreactivity. *J. Phys. Chem. C* **2011**, *115*, 9136–9145. [CrossRef]

23. Xiang, Q.; Yu, J. Graphene-based photocatalysts for hydrogen generation. *J. Phys. Chem. Lett.* **2013**, *4*, 753–759. [CrossRef] [PubMed]

24. Zhang, N.; Xu, Y. Aggregation- and leaching-resistant, reusable, and multifunctional Pd@CeO$_2$ as a robust nanocatalyst achieved by a hollow core-shell strategy. *Chem. Mater.* **2013**, *25*, 1979–1988. [CrossRef]

25. Zong, X.; Yan, H.; Wu, G.; Ma, G.; Wen, F.; Wang, L.; Li, C. Enhancement of photocatalytic H$_2$ evolution on CdS by loading MoS$_2$ as cocatalyst under visible light irradiation. *J. Am. Chem. Soc.* **2008**, *130*, 7176–7177. [CrossRef] [PubMed]

26. Inoue, Y. Photocatalytic water splitting by RuO$_2$-loaded metal oxides and nitrides with d^0- and d^{10}-related electronic configurations. *Energy Environ. Sci.* **2009**, *2*, 364–386. [CrossRef]

27. Asai, R.; Nemoto, H.; Jia, Q.; Saito, K.; Iwase, A.; Kudo, A. A visible light responsive rhodium and antimony-codoped SrTiO$_3$ powdered photocatalyst loaded with an IrO$_2$ cocatalyst for solar water splitting. *Chem. Commun.* **2014**, *50*, 2543–2546. [CrossRef] [PubMed]

28. Higashi, M.; Domen, K.; Abe, R. Highly stable water splitting on oxynitride TaON photoanode system under visible light irradiation. *J. Am. Chem. Soc.* **2012**, *134*, 6968–6971. [CrossRef] [PubMed]

29. Wang, D.; Li, R.; Zhu, J.; Shi, J.; Han, J.; Zong, X.; Li, C. Photocatalytic water oxidation on BiVO$_4$ with the electrocatalyst as an oxidation cocatalyst: Essential relations between electrocatalyst and photocatalyst. *J. Phys. Chem. C* **2012**, *116*, 5082–5089. [CrossRef]

30. Wang, S.; Qian, H.; Hu, Y.; Dai, W.; Zhong, Y.; Chen, J.; Hu, X. Facile one-pot synthesis of uniform TiO$_2$-Ag hybrid hollow spheres with enhanced photocatalytic activity. *Dalton Trans.* **2013**, *42*, 1122–1128. [CrossRef] [PubMed]

31. Grzelczak, M.; Zhang, J.; Pfrommer, J.; Hartmann, J.; Driess, M.; Antonietti, M.; Wang, X. Electro-and photochemical water oxidation on ligand-free Co$_3$O$_4$ nanoparticles with tunable sizes. *ACS Catal.* **2013**, *3*, 383–388. [CrossRef]

32. Liu, L.; Ji, Z.; Zou, W.; Gu, X.; Deng, Y.; Gao, F.; Tang, C.; Dong, L. In situ loading transition metal oxide clusters on TiO$_2$ nanosheets as co-catalysts for exceptional high photoactivity. *ACS Catal.* **2013**, *3*, 2052–2061. [CrossRef]

33. Luo, X.; Deng, F.; Min, L.; Luo, S.; Guo, B.; Zeng, G.; Au, C. Facile one-step synthesis of inorganic-framework molecularly imprinted TiO$_2$/WO$_3$ nanocomposite and its molecular recognitive photocatalytic degradation of target contaminant. *Environ. Sci. Technol.* **2013**, *47*, 7404–7412. [PubMed]

34. Son, J.; Chattopadhyay, J.; Pak, D. Electrocatalytic performance of Ba-doped TiO$_2$ hollow spheres in water electrolysis. *Int. J. Hydrog. Energy* **2010**, *35*, 420–427. [CrossRef]

35. Uddin, M.; Nicolas, Y.; Olivier, C.; Toupance, T.; Müller, M.; Kleebe, H.; Rachut, K.; Ziegler, J.; Klein, A.; Jaegermann, W. Preparation of RuO$_2$/TiO$_2$ mesoporous heterostructures and rationalization of their enhanced photocatalytic properties by band alignment investigations. *J. Phys. Chem. C* **2013**, *117*, 22098–22110. [CrossRef]

36. Sarkar, D.; Ghosh, C.; Mukherjee, S.; Chattopadhyay, K. Three dimensional Ag$_2$O/TiO$_2$ type-II (p-n) nanoheterojunctions for superior photocatalytic activity. *ACS Appl. Mater. Inter.* **2013**, *5*, 331–337. [CrossRef] [PubMed]

37. Yu, J.; Yu, H.; Cheng, B.; Zhao, X.; Yu, J.; Ho, W. The effect of calcination temperature on the surface microstructure and photocatalytic activity of TiO$_2$ thin films prepared by liquid phase deposition. *J. Phys. Chem. B* **2003**, *107*, 13871–13879. [CrossRef]

38. Ren, W.; Ai, Z.; Jia, F.; Zhang, L.; Fan, X.; Zou, Z. Low temperature preparation and visible light photocatalytic activity of mesoporous carbon-doped crystalline TiO$_2$. *Appl. Catal. B Environ.* **2007**, *69*, 138–144. [CrossRef]

39. Zhang, H.; Wang, G.; Chen, D.; Lv, X.; Li, J. Tuning photoelectrochemical performances of Ag-TiO$_2$ nanocomposites via reduction/oxidation of Ag. *Chem. Mater.* **2008**, *20*, 6543–6549. [CrossRef]

40. Zhou, W.; Liu, H.; Wang, J.; Liu, D.; Du, G.; Cui, J. Ag$_2$O/TiO$_2$ nanobelts heterostructure with enhanced ultraviolet and visible photocatalytic activity. *ACS Appl. Mater. Interfaces* **2010**, *2*, 2385–2392. [CrossRef] [PubMed]